Approaches for theoretical and experimental determinations of K-shell decay rates and fluorescence yields in Ge

J. M. Sampaio,[1] T. I. Madeira,[1] J. P. Marques,[1] F. Parente,[2] A. M. Costa,[1] P. Indelicato,[3] J. P. Santos,[2] M.-C. Lépy,[4] and Y. Ménesguen[4]

[1]*Centro de Física Atómica, CFA, Departamento de Física, Faculdade de Ciências, FCUL, Universidade de Lisboa, Campo Grande, Ed. C8, 1749-016, Lisboa, Portugal*

[2]*Centro de Física Atómica, CFA, Departamento de Física, Faculdade de Ciências e Tecnologia, FCT, Universidade Nova de Lisboa, 2829-516, Caparica, Portugal*

[3]*Laboratoire Kastler Brossel, École Normale Supérieure, CNRS, Université Pierre et Marie Curie, Paris 6, Case 74; 4, place Jussieu, 75252, Paris Cedex 05, France*

[4]*CEA, LIST, Laboratoire National Henri Becquerel CEA Saclay, F-91191, Gif-sur-Yvette Cedex, France*

(Received 6 November 2013; published 23 January 2014)

Fluorescence yields are one of the fundamental parameters in atomic physics and related areas. Despite the increase of experimental work in the last decade, to obtain values of K-shell fluorescence yields available data are scarce or outdated for many elements. The available theoretical results cannot fill the gap since quite often they are derived from semi-empirical calculations based on old models. This is the case of Ge that has many applications in science. In this work, we present the results of a collaboration between an experimental and a theoretical group to obtain the decay rates and fluorescence yields for Ge. The calculations were performed within the Dirac-Fock method, including relativistic and QED corrections, using a state-of-the-art approach. The experimental work was carried out at the SOLEIL synchrotron and the fluorescence yields were measured by two distinct methods: the reflection geometry method and the escape peak method. The results show a very good agreement between the experiment and theory (1.1%), well within the experimental uncertainty (2.4%).

DOI: 10.1103/PhysRevA.89.012512 PACS number(s): 32.70.Fw, 32.10.−f, 31.15.−p

I. INTRODUCTION

The creation of a hole in the atomic K shell by electrons, photons, protons, and ions, leads to a rearrangement of the electronic structure of the atom through the filling of the vacancy by an electron from a higher shell, shifting the hole to that shell. The difference between the binding energies of the two shells is transferred to another bound electron that is subsequently ejected (radiationless transition) or is released as an x-ray photon (radiative transition). In the K-shell radiationless transitions (or Auger transitions) the vacancy can only be filled by electrons from higher shells (and not by an electron of the same shell), resulting in an ion with two vacancies in those shells. K-shell radiative transitions are labeled, according to the Siegbahn notation, as $K\alpha$ or $K\beta$ transitions, depending on the final hole shell (α for the L shell, and β for the M and N shells, according to the International Union of Pure and Applied Chemistry (IUPAC) denomination [1]). Following the same reasoning, radiationless transitions are described by identifying the final holes' subshells. For example, the process that involves a transition of the initial hole in the L_2 subshell, with the ejection of an M_1 electron is identified as the K-L_2M_1 transition. The correspondence between the Siegbahn, IUPAC, and nl_j electron configuration (EC) notations is presented in Table I.

The knowledge of accurate values of decay rates associated with these transitions is fundamental for the characterization of the atomic elements in materials and the interaction of ionizing radiation with them. One of the most important parameters is the fluorescence yield, defined as the relative probability that a hole in a given shell or subshell is filled through a radiative transition. Fluorescence yields are necessary in many areas related to physics, namely in the quantitative analysis of samples in x-ray spectroscopy to derive the energy-absorption coefficients related to dosimetric quantities, in plasma physics, to characterize the emitted x-ray spectra, and in astrophysics to compute the emission and absorption lines in stellar objects.

A large number of works dealing with the experimental, theoretical, and empirical evaluation of x-ray fluorescence yields for different elements has been published by several authors. Calculations in the late 1960s and early 1970s were essentially nonrelativistic [2–5], although, already in 1970, there was a relativistic calculation by Bhalla of M-shell radiative transition probabilities using the Dirac-Hartree-Slater (DHS) approach [6]. In the early 1980s, Chen *et al.* performed a series of relativistic calculations of K- [7], L- [8], and M-shell [9,10] radiationless transitions for several elements from $Z = 18$ to $Z = 96$, also based on the DHS approach. They showed that relativistic effects in individual transitions are between 10% to 50% relative to the nonrelativistic values. These results also pointed out the importance of going beyond an independent particle model towards a multiconfiguration calculation.

In the last decade there was an increase of high precision measurements of K-shell fluorescence yields [11–13] and a few calculations [14,15] for several elements such as K, Ca, Zn, Cd, and Hg. Despite these efforts, the available experimental and theoretical fluorescence yield data for some elements are scarce or were obtained several decades ago, calling for further efforts to update values with high precision measurements and state-of-the-art calculations. One of these elements is germanium, for which available data include the experimental works of Pahor *et al.* [16], Hartl *et al.* [17], Casnati *et al.* [18], Brunner [19], Pious *et al.* [20], and Durak *et al.* [21]; the semi-empirical data of Bambynek *et al.* [5], Krause [22] and Hubbell *et al.* [23]; and the nonrelativistic calculations of

TABLE I. Correspondence between Siegbhan, IUPAC [1], and nl_j electron configuration (EC) notations for radiative transitions, where n is the principal quantum number, l is the orbital angular momentum, and j is the total angular momentum quantum number.

Siegbahn		IUPAC	EC
K_α	$K\alpha_3$	K–L_1	$1s_{1/2}$–$2s_{1/2}$
	$K\alpha_2$	K–L_2	$1s_{1/2}$–$2p_{1/2}$
	$K\alpha_1$	K–L_3	$1s_{1/2}$–$2p_{3/2}$
$K\beta$	$K\beta_3$	K–M_2	$1s_{1/2}$–$3p_{1/2}$
	$K\beta_1$	K–M_3	$1s_{1/2}$–$3p_{3/2}$
	$K\beta_5^{II}$	K–M_4	$1s_{1/2}$–$3d_{3/2}$
	$K\beta_5^{I}$	K–M_5	$1s_{1/2}$–$3d_{5/2}$
	$K\beta_2^{II}$	K–N_2	$1s_{1/2}$–$4p_{1/2}$
	$K\beta_2^{I}$	K–N_3	$1s_{1/2}$–$4p_{3/2}$

McGuire [3], Walters *et al.* [4], and Kostroun *et al.* [24]. Hence, the most recent experimental data were obtained 12 years ago and the last theoretical values were published more than 40 years ago. Significant discrepancies were observed between these data, and new careful study with today's facilities should improve the fluorescence yield knowledge. Germanium is used as a semiconductor in various electronic devices and in nuclear and particle physics detectors, in solar cell applications, and in chemistry to produce organometallic compounds. The isotopes of Ge are the daughter elements of 16 of the 33 known isotopes of arsenic [25], as, for instance, the ^{74}As isotope (a positron emitter) used to locate tumours [26].

In this work, we present the results of a collaboration between one experimental and one theory group to obtain very precise results for K-shell decay rates and fluorescence yield in Ge.

Theoretical fluorescence yields were derived from state-of-the-art calculations of decay rates, employing the multiconfiguration Dirac-Fock (MCDF) approach to obtain the radiative and radiationless transition rates for Ge following a K-shell vacancy creation, while experimental fluorescence yields were measured, with high precision, at the metrology beamline of the SOLEIL synchrotron using two different methods: the reflection geometry method and the escape peak method.

The article is organized as follows. A brief explanation of the principles employed in the MCDF calculations of decay rates and fluorescence yields is given in Sec. II and the experimental methodologies are described in Sec. III. Experimental and theoretical results are presented and discussed in Sec. IV. Comparisons to previous data are done in Sec. V together with conclusions from the obtained results.

II. DECAY RATES AND YIELDS

Wave functions and binding energy values, as well as K-shell radiative and radiationless decay rates for Ge, were calculated using the relativistic general purpose MCDF code developed by Desclaux and Indelicato [27,28]. The code was used in the single-configuration approach, with the Breit interaction and the vacuum polarization terms included in the self-consistent field calculation, and other QED effects included as perturbations. A detailed description of the Hamiltonian and wave functions can be obtained in [29–32].

A. Relativistic calculations

Radiative decay rates were calculated using the relativistic formulas implemented in the MCDF program [32–35]. The so-called optimized levels (OL) method was used to calculate the wave functions and energies of the levels involved in all possible transitions, using the full relaxation of both initial and final states, hence providing more accurate energies and wave functions. Since the spin-orbitals of the initial and final levels were optimized separately, they are not orthogonal. To deal with the nonorthogonality of the wave functions, the code uses the formalism described by Löwdin [36].

In what concerns the radiationless transitions, we assumed a two-step process, in which the decay is treated independently from the primary ionization. Accordingly, the primary ejected electron in the inner-shell ionization process does not interact with the Auger electron and the interaction of the core hole state with the continuum electron is weak. Hence, the radiationless transition probabilities can be calculated from perturbation theory. Initial-state wave functions were generated for configurations that contain one initial inner-shell vacancy while final state wave functions were generated for configurations that contain two higher shell vacancies. Continuum-state wave functions were obtained by solving the Dirac-Fock equations with the same atomic potential of the initial state, normalized to represent one ejected electron per unit energy. Radiationless rates were, however, calculated using the correct transition energies obtained in previous independent calculations of initial and final state wave functions and eigenvalues [37–39].

To keep consistency between the radiative and radiationless calculations, multiconfiguration wave functions beyond intermediate coupling were not employed because the approximation used for the evaluation of the Auger rate cannot be used in an optimized level calculation with correlation orbitals.

B. K-shell fluorescence yield

Although the general definition of the fluorescence yield is well known, special attention must be devoted to the details of its calculation. The fluorescence yield, for the K shell, is defined as the relative probability that a K-shell vacancy is filled through a radiative transition, i.e.,

$$\omega_K = \frac{\Gamma^{\mathrm{R}}}{\Gamma} = \frac{\Gamma^{\mathrm{R}}}{\Gamma^{\mathrm{R}} + \Gamma^{\mathrm{NR}}}, \tag{1}$$

where Γ, Γ^{R}, Γ^{NR} are the total, radiative, and radiationless widths, respectively, of the initial hole level in the K shell.

Assuming that the initial K-shell multiplet levels, identified by the total angular momentum J_i, are statistically populated, and considering the relation between the natural widths and the decay rates, Eq. (1) may be written as

$$\omega_K = \frac{\sum_i (2J_i + 1) W_i^{\mathrm{R}}}{\sum_i (2J_i + 1)\left(W_i^{\mathrm{R}} + W_i^{\mathrm{NR}}\right)}, \tag{2}$$

where W_i^{R} and W_i^{NR} stand for the radiative and radiationless decay rates of the initial hole level i in the K shell.

III. MEASUREMENTS OF FLUORESCENCE YIELDS

The measurements were performed at the metrology beamline of the SOLEIL synchrotron facility. The "hard x-rays" branch is equipped with a double Si (111) crystal monochromator, providing monoenergetic photons in the 3.5 to 35 keV energy range. An important part in the experimental setup is the energy calibration of the resulting photons. Tunable and monochromatic x-ray sources are ideal for this purpose, and an accurate calibration is obtained by an energy scanning around the electron binding energies [40] of the different elements inserted in the photon path. This makes possible establishing the link between the monochromator angle and the energy of the photons E with an associated uncertainty of $10^{-5}E$. Beam stability and purity must also be ensured: Here, the photon flux intensity stability is better than 0.3% due to the top-up mode of the synchrotron, and high-order harmonics are rejected by a small detuning of the second crystal (necessary only for energies below 7 keV).

The experimental methodology is carried out in two steps. (i) Accurate values of the Ge mass-attenuation coefficients are measured, using procedures already optimized for similar measurements [41]. Special care is taken around the K-shell binding energy of Ge, and for the energy of its characteristic x-rays. (ii) The K-shell fluorescence yields are determined using two experimental approaches as follows.

(1) In a traditional reflection configuration, where a germanium target is installed at 45° both from the incident radiation and from an energy-dispersive detector.

(2) Without any target, using only the escape peaks of a high purity germanium (HPGe) detector, evaluating the escape-peak to parent-peak intensity ratio which directly depends on the fluorescence yield [13,19,42].

A. Mass-attenuation coefficients

A very convenient way to measure mass-attenuation coefficients is in transmission mode, using a monochromatic parallel photon beam under normal incidence to the sample with thickness x, recording the photon flux intensity in front of the sample I_0, and just behind it I [43]. For monochromatic photons with energy E, the overall beam attenuation follows the Beer-Lambert law

$$I = I_0 \exp\left[-\frac{\mu}{\rho}(E)\rho x\right] = I_0 \exp\left[-\frac{\mu}{\rho}(E)\frac{M}{A}\right], \quad (3)$$

where $\mu(E)$ is the linear attenuation coefficient of the sample material and ρ is its mass per unit volume; the mass-attenuation coefficient is defined by $(\mu/\rho)(E)$. For a good measurement, i.e., with an uncertainty budget as low as possible, one has to accurately measure I and I_0, but also to know the characteristics of the sample such as its thickness and density, or, equivalently, its area A and mass M. A study of the uncertainty budget associated with the counting statistics led Nordfors *et al.* [44] to establish a criterion to minimize the statistical uncertainty. The best results are obtained for samples with thicknesses satisfying $2 \leqslant \ln(I_0/I) \leqslant 4$. For the energy range of interest, the selected target is a 4×4 mm^2 area and 50-μm thickness Ge foil (99.999% purity) purchased from Goodfellow®.

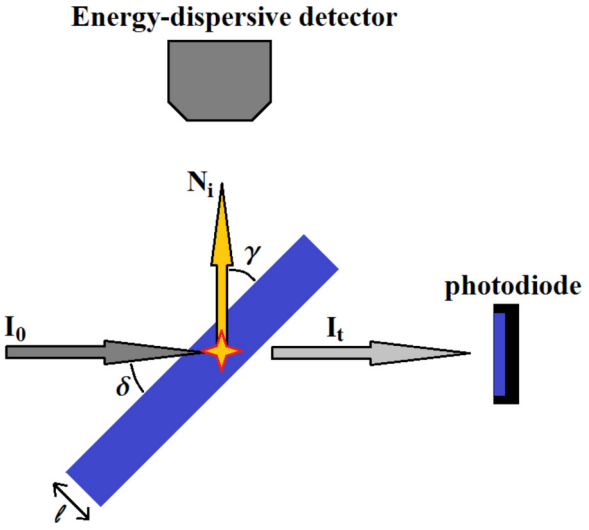

FIG. 1. (Color online) Geometry of the experimental setup.

B. Reflection geometry method

In the reflection geometry (see Fig. 1), the monochromatic photon beam, with energy E_0 is attenuated in the target material, according to the linear attenuation coefficient $\mu_0 = \mu(E_0)$, and interacts at depth x, by photoelectric effect in the K shell with probability τ_K. Consecutive electronic rearrangement produces characteristic x rays with energy E_X ($X = \alpha$ for a $K\alpha$ transition and $X = \beta$ for a $K\beta$ transition), according to the partial fluorescence yield of the target element ω_{KX}. The external detector can record these emerging photons, after their attenuation through the material, depending on the relevant total attenuation coefficient $\mu_X = \mu(E_X)$; the elemental number of events in the full-energy peak corresponding to energy E_X is proportional to the elemental detection solid angle $d\Omega$ and to the full-energy peak efficiency ε_X,

$$dN_X = I_0 \exp\left[-\frac{\mu_0 x}{\sin\gamma}\right] \times \tau_K \frac{dx}{\sin\gamma}\omega_{KX} \exp\left[-\frac{\mu_X x}{\sin\delta}\right]\frac{d\Omega}{4\pi}\varepsilon_X. \quad (4)$$

If the target is situated at the angles $\gamma = \delta$ from both the incident photon beam and the detector entrance window, this simplifies to

$$dN_X = I_0\tau_K\omega_{KX} \exp\left[-\frac{(\mu_0+\mu_X)x}{\sin\gamma}\right]\frac{dx}{\sin\gamma}\frac{d\Omega}{4\pi}\varepsilon_X. \quad (5)$$

Integrating this equation on the target thickness ℓ and the detection solid angle gives N_X, the number of counts recorded in the full-energy peak corresponding to the characteristic energy E_X,

$$N_X = I_0\tau_K\omega_{KX}\frac{1-\exp\left[-\frac{\mu_0+\mu_X}{\sin\gamma}\ell\right]}{\mu_0+\mu_X}\frac{\Omega}{4\pi}\varepsilon_X. \quad (6)$$

The partial K-shell fluorescence yield is then

$$\omega_{KX} = \frac{4\pi}{\Omega}\frac{N_X}{\varepsilon_X}\frac{1}{I_0\tau_K}\frac{\mu_0+\mu_X}{1-\exp\left[-\frac{\mu_0+\mu_X}{\sin\gamma}\ell\right]}. \quad (7)$$

In this experimental setup, the germanium target is at 45° from the incident beam, and a photodiode is installed behind it. This photodiode records the transmitted photon flux during the spectrum acquisition, thus, knowing the target attenuation coefficients, the incident photon beam intensity is derived. An energy-dispersive detector (silicon drift detector) is positioned at 45° from the target and 90° from the incident beam direction, to record the fluorescence spectra.

As previously mentioned, different parameters must be carefully checked to ensure high-quality measurements, with low uncertainties: the photon beam quality, target characteristics, and transmission measurements using the photodiode. The required attenuation coefficients are obtained from the present experimental results. Moreover, the energy-dispersive detector must be efficiency calibrated and a collimator is used to accurately determine the detection solid angle. The fluorescence net peak area N_X is determined using a dedicated routine from ROOT [45].

C. Escape peak method

In the escape peak approach the energy-dispersive detector is a high purity germanium detector (HPGe), the target being also a detector. Therefore, the above equations simplify and the target thickness, detector efficiency, and geometrical solid angle are no longer involved. The energy dispersive detector records the full-energy peak corresponding to the incident photon flux, with net area N_0, and the associated Ge $K\alpha$ and $K\beta$ escape peaks rising at $E_0 - 9.88$ keV and $E_0 - 10.98$ keV, with respective net areas N_a and N_b. The ratio of the escape peak N_X to the sum of the three peaks is [19,42]

$$\eta_X = \frac{N_X}{N_0 + N_a + N_b} = \frac{\omega_{KX}}{2}\frac{\tau_K}{\mu_0}\left[1 - \frac{\mu_X}{\mu_0}\ln\left(1 + \frac{\mu_0}{\mu_X}\right)\right]. \tag{8}$$

Thus,

$$\omega_{KX} = 2\eta_X\frac{\mu_0}{\tau_K}\left[1 - \frac{\mu_X}{\mu_0}\ln\left(1 + \frac{\mu_0}{\mu_X}\right)\right]. \tag{9}$$

Figure 2 shows an example of the spectrum obtained with 14-keV parent peak (incidence energy) and the associated $K\alpha$ and $K\beta$ germanium escape peaks. The peaks of interest are processed using the COLEGRAM software [46], and the required attenuation coefficients are taken from the first method of the experiment.

IV. RESULTS AND DISCUSSION

A. Calculation of decay rates and fluorescence yields

In Table II, we present the computed radiative decay rates for Ge, for all transitions from K-shell holes to higher subshells, as a function of the initial state total angular momentum J_i (in a.u.). These decay rates include the sum over electric and magnetic multipoles up to rank 3. The first column identifies the final state subshell hole, and in the sixth column we list, in percentage, the contribution of each subshell to the total radiative decay rate. The theoretical radiationless transition probabilities for Ge and, for each initial state, the total angular momentum J_i (in a.u.) are listed in Table III. They are the result of the sum over the initial state for a given angular momentum and the final state angular momentum J_f. The values shown also include the statistical weight factor $(2J_i + 1)$.

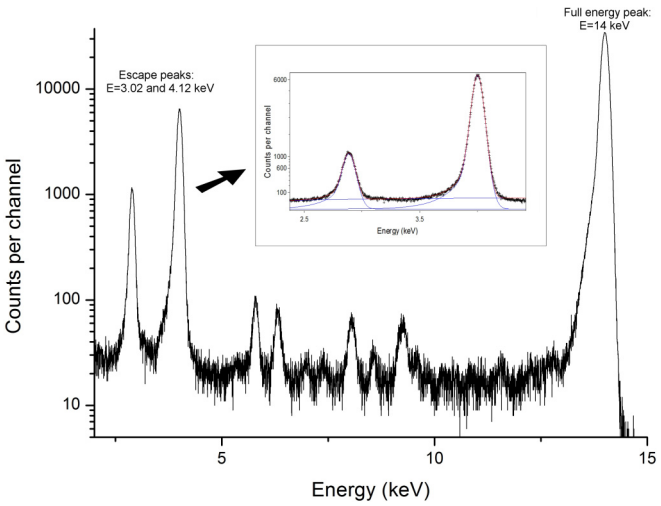

FIG. 2. (Color online) Spectrum obtained with 14-keV incident energy with detailed processing of the escape peak's area. Blue lines stand for the fitting contributions and red line for the fitting line.

In the sixth column we list, as a percentage of the total, the contribution of each group to the total decay rate. We conclude that the contribution of the L shell (L_1, L_2, and L_3 subshells) is about 98.6%, i.e., the computational effort to calculate the contribution for the M and N shells represents a contribution of only 1.4% to the total value. From these rates we derive a K-shell fluorescence yield value of $\omega_K = 0.547$. Although there is no reliable way to estimate the uncertainty of these kinds of calculations that involve relativistic operators, by studying the convergence and the influence of the different contributions we estimate that the uncertainty of the obtained ω_K value is 0.005, i.e., less than 1%.

B. Measurements of the fluorescence yield

The best way to perform traceable measurements is to weigh the sample and measure its area to derive the M/A value with low associated uncertainties. The sample is weighed with a relative uncertainty of 0.03%, and its area is measured with a vision machine associated with a dedicated pictures processing software leading to a relative uncertainty of 0.2%.

The transmission measurement is performed using a collimated photon beam, with square aperture 2×2 mm, to ensure that the involved area is representative of the sample average thickness. The measurement sequence consists of a loop on energies starting with highest energies and going down. For each energy, the photon flux is measured doing an average of at least five current values recorded with an AXUV diode in two configurations: with the sample and without the sample. Experimental data resulting from this scan are spaced every 50 eV between 35 and 7 keV. Then additional measurements are done between 12 and 11.155 keV every 10 eV and every eV between 11.154 and 11.055 keV. The measurements results (about 730 experimental values) are presented in Fig. 3, with a magnification of the K-shell edge fine structures. In

TABLE II. K-shell radiative decay rates for Ge as a function of the initial state total angular momentum J_i (in a.u.). The first column identifies the final state subshell vacancy. The total value for each final state shell, and for each J_i, takes into account the statistical weight of each J_i.

	$J_i = 1/2$	$J_i = 3/2$	$J_i = 5/2$	Total	%
L_1	2.05×10^{-7}	1.89×10^{-7}	1.30×10^{-7}	1.94×10^{-6}	<0.001
L_2	4.45×10^{-2}	2.95×10^{-2}	2.34×10^{-2}	3.47×10^{-1}	29.645
L_3	6.71×10^{-2}	6.75×10^{-2}	4.50×10^{-2}	6.74×10^{-1}	57.610
M_1	3.42×10^{-8}	3.35×10^{-8}	2.25×10^{-8}	3.38×10^{-7}	<0.001
M_2	4.86×10^{-3}	5.01×10^{-3}	3.23×10^{-3}	4.92×10^{-2}	4.200
M_3	9.39×10^{-3}	9.64×10^{-3}	6.56×10^{-3}	9.67×10^{-2}	8.265
M_4	8.36×10^{-6}	1.20×10^{-5}	3.47×10^{-6}	8.54×10^{-5}	0.007
M_5	1.26×10^{-5}	9.03×10^{-6}	1.06×10^{-5}	1.25×10^{-4}	0.011
N_1	2.98×10^{-9}	2.92×10^{-9}	1.95×10^{-9}	2.93×10^{-8}	<0.001
N_2	2.85×10^{-5}	3.25×10^{-4}	1.28×10^{-6}	1.37×10^{-3}	0.117
N_3	3.78×10^{-4}	8.01×10^{-5}	1.03×10^{-4}	1.69×10^{-3}	0.145
Total	2.52×10^{-1}	4.48×10^{-1}	4.69×10^{-1}	1.17×10^{0}	

addition to the target thickness, the uncertainty budget also includes the photon flux I and I_0 contributions and the final relative combined standard uncertainty associated with the mass attenuation coefficients is 0.5%. The relative differences between our experimental values μ_{LNHB} and the tabulated values [47,48] μ_{Tab} defined by

$$R_{\mathrm{Tab}} = \frac{\mu_{\mathrm{LNHB}} - \mu_{\mathrm{Tab}}}{\mu_{\mathrm{Tab}}} \times 100 \qquad (10)$$

are presented in Fig. 4. It shows a clear tendency above the K-shell edge where the present values are larger by a few percent. Above 20 keV no trend is evident.

Figure 5 shows the values derived for the partial K-shell fluorescence yields $\omega_{K\alpha}$ and $\omega_{K\beta}$ with their mean values and standard deviation for $k = 1$ using both experimental approaches. The results from the reflection method are presented on the top panel and correspond to eight incident energies in the 11.5- to 15-keV energy range. With this method, the total K-shell fluorescence yield is found to be $\omega_K = 0.554(8)$.

The results from the escape peak method are obtained with seven incident energies in the 12.2- to 14-keV energy range, and are presented in the bottom panel of Fig. 5. In this case, the relative standard deviation is larger (about 2.5% for the partial values, instead of 1.4% in the reflection mode), and the total K-shell fluorescence yield is found to be $\omega_K = 0.552(13)$. Both series of results are fully consistent, and the final experimental value is obtained as the weighted mean, which gives $\omega_K = 0.553(13)$.

C. Discussion of the results

Table IV reports the the K-shell fluorescence yield values for Ge (experimental and theoretical) obtained in this work, together with the experimental, theoretical, and semi-empirical values obtained by other authors. A very good agreement between our experimental and theoretical results, better than 1.1 %, is evident. This agreement mutually validates our results.

Regarding the available experimental results, we notice that the ones by Pahor *et al.* [16], Hartl *et al.* [17], and Brunner [19] agree with our results; the relative differences to the measured value in this work being 0.1%, 1.5%, and 3.8%, respectively.

TABLE III. K-shell radiationless decay rates for Ge as a function of the initial state total angular momentum J_i (in a.u.). L_1-$L_{1,\ldots,3}M_{1,\ldots,5}N_{1,\ldots,3}$ means that after the radiationless transition the atom with an initial K-shell vacancy ends up with a vacancy in the L_1 subshell and another vacancy in either of the $L_{1,\ldots,3}$, $M_{1,\ldots,5}$, and $N_{1,\ldots,3}$ shells. The total value for each final state shell, and for each J_i, takes into account the statistical weight of each J_i.

	$J_i = 1/2$	$J_i = 3/2$	$J_i = 5/2$	Total	%
L_1-$L_{1,\ldots,3}M_{1,\ldots,5}N_{1,\ldots,3}$	3.43×10^{-2}	3.43×10^{-2}	2.29×10^{-2}	3.43×10^{-1}	35.378
L_2-$L_{23}M_{1,\ldots,5}N_{1,\ldots,3}$	4.42×10^{-2}	4.49×10^{-2}	3.01×10^{-2}	4.48×10^{-1}	46.259
L_3-$L_3M_{1,\ldots,5}N_{1,\ldots,3}$	1.73×10^{-2}	1.61×10^{-2}	1.09×10^{-2}	1.64×10^{-1}	16.960
M_1-$M_{1,\ldots,5}N_{1,\ldots,3}$	5.10×10^{-4}	5.24×10^{-4}	3.51×10^{-4}	5.22×10^{-3}	0.539
M_2-$M_{2,\ldots,5}N_{1,\ldots,3}$	6.82×10^{-4}	7.06×10^{-4}	4.73×10^{-4}	7.03×10^{-3}	0.725
M_3-$M_{3,\ldots,5}N_{1,\ldots,3}$	1.47×10^{-4}	1.23×10^{-4}	8.03×10^{-5}	1.27×10^{-3}	0.131
M_4-$M_{45}N_{1,\ldots,3}$	4.92×10^{-6}	4.60×10^{-6}	2.40×10^{-6}	4.27×10^{-5}	0.004
M_5-$M_5N_{1,\ldots,3}$	2.80×10^{-6}	2.40×10^{-6}	1.17×10^{-6}	2.22×10^{-5}	0.002
N_1-$N_{1,\ldots,3}$	1.41×10^{-6}	1.38×10^{-6}	1.04×10^{-6}	1.46×10^{-5}	0.002
N_2-N_{23}	9.38×10^{-10}	1.27×10^{-7}	1.16×10^{-9}	5.16×10^{-7}	<0.001
N_3-N_3	6.52×10^{-8}	3.26×10^{-9}	1.34×10^{-7}	9.49×10^{-7}	<0.001
Total	1.94×10^{-1}	3.86×10^{-1}	3.89×10^{-1}	9.69×10^{-1}	

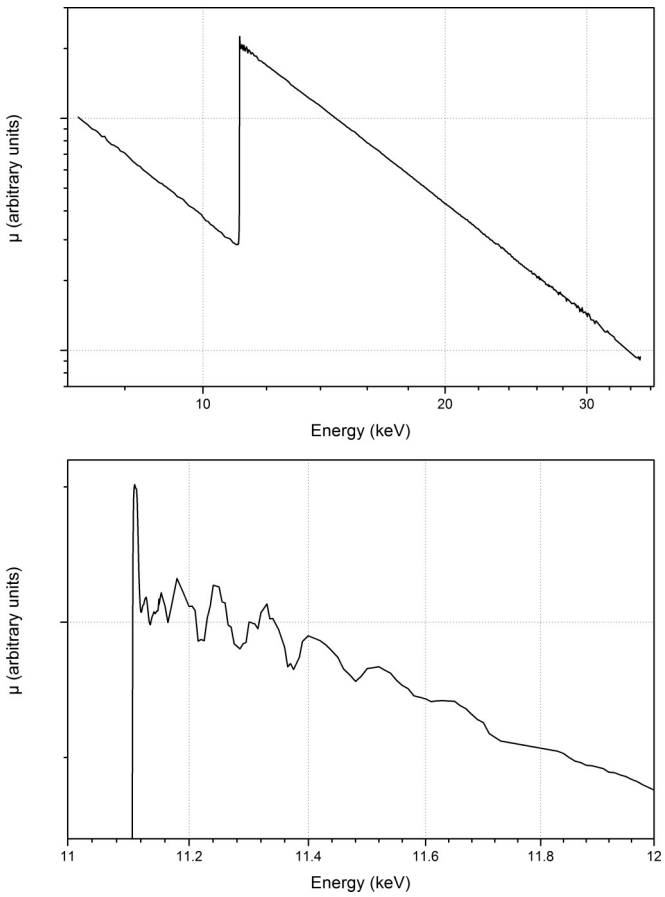

FIG. 3. Mass-attenuation coefficients of Ge measured between 7 and 35 keV (top panel) and near edge fine structures (bottom panel).

Although the other experimental results lie outside the region defined by the experimental uncertainty of our measurements, their error bars touch that region.

Considering the available theoretical and semi-empirical results, only the McGuire [3], Kostroun *et al.* [24], and Bambynek *et al.* [5] are in agreement with our results; their relative differences to the measured value in this work being 1.0%, 1.5%, and 2.4%, respectively. The remaining values by Krause [22], Hubbell *et al.* [23], and Walters *et al.* [4] lie outside the above-mentioned region.

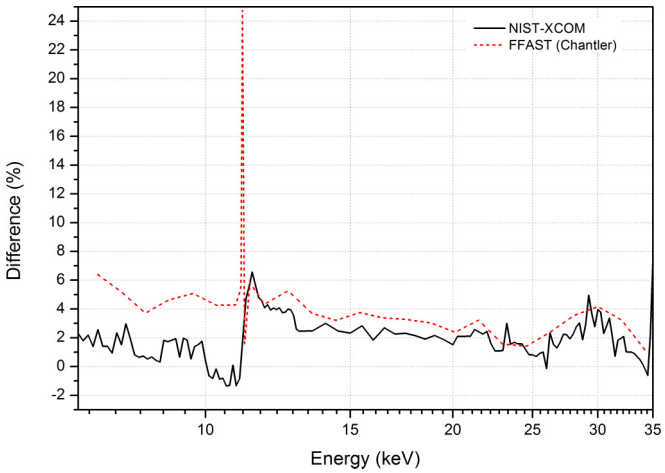

FIG. 4. (Color online) Relative differences R_{Tab} between our experimental values μ_{LNHB} and the tabulated values [47,48].

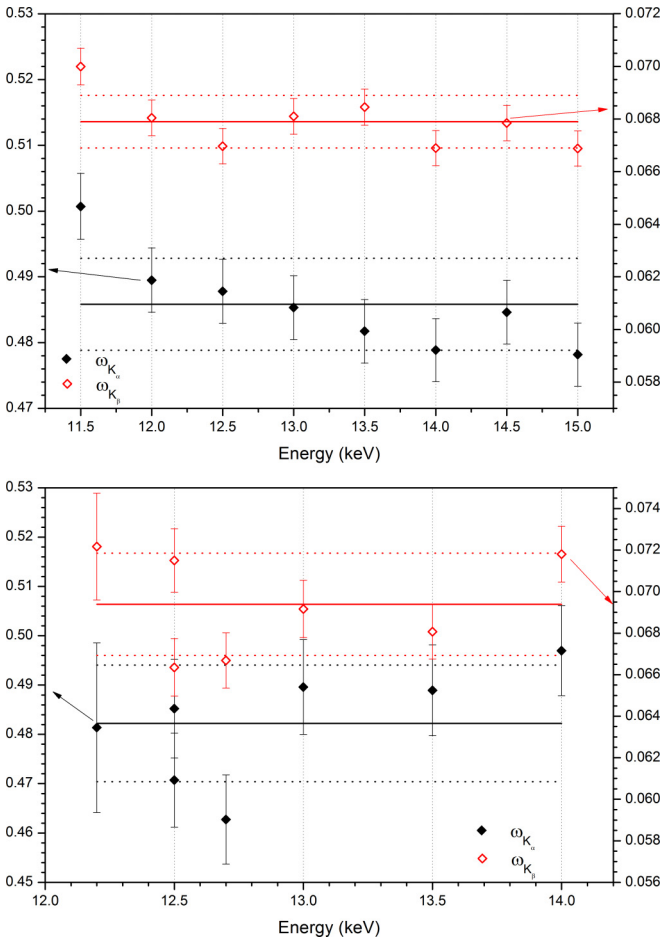

FIG. 5. (Color online) Ge partial K-shell fluorescence yields in the reflection setup measurement (top panel) and escape peak method (bottom panel). Black diamonds ♦ (Kα fluorescence yields) refer to the left vertical scale and red diamonds ⋄ (Kβ fluorescence yields) refer to the right one.

TABLE IV. K-shell fluorescence yield values for Ge.

	Expt.	Theo.	Semi-emp.
This work	0.553 ± 0.013	0.547	
Pahor *et al.* [16]	0.554 ± 0.003		
McGuire *et al.* [3]		0.558	
Kostroun *et al.* [24]		0.545	
Walters *et al.* [4]		0.534	
Bambynek *et al.* [5]			0.540
Hartl *et al.* [17]	0.561 ± 0.015		
Krause [22]			0.535
Casnati *et al.* [18]	0.549 ± 0.011		
Brunner [19]	0.532 ± 0.016		
Pious *et al.* [20]	0.538 ± 0.029		
Hubbell *et al.* [23]			0.523
Durak *et al.* [21]	0.537 ± 0.03		

V. CONCLUSION

The available experimental, theoretical, and semi-empirical values of K-shell fluorescence yields for Ge are scarce; moreover relative uncertainties associated to experimental values differ by a factor of 10. There is a case to be made that 50-year-old results should be reexamined with new experimental and theoretical techniques. In this work, we present the results of a collaboration between an experimental and a theoretical group, within the International Initiative on an x-ray fundamental parameters framework, to obtain decay rates and fluorescence yields for Ge.

The Dirac-Fock method, including relativistic and QED corrections, has been used to obtain the wave functions and binding energy values, as well as K-shell radiative and radiationless decay rates for Ge. This approach leads to the K-shell fluorescence yield value of 0.547, with an uncertainty estimate of 1%.

The experimental value of $\omega_K = 0.553$, with an uncertainty 2.4%, was obtained using two distinct methods in the SOLEIL synchrotron facility: the reflection geometry method and the escape peak method.

The results obtained in this work show a very good agreement between the experiment and theory (1.1%), and contribute to establishing a benchmark for the Ge K-shell fluorescence yield value.

ACKNOWLEDGMENTS

This research was supported in part by Fundação para a Ciência e a Tecnologia (FCT), Portugal, through Projects No. PEstOE/FIS/UI0303/2011 and No. PTDC/FIS/117606/2010, financed by the European Community Fund FEDER through the COMPETE. We also thank the Allianz Program of the Helmholtz Association, Contract No. EMMI HA-216 "Extremes of Density and Temperature: Cosmic Matter in the Laboratory." T.I.M. acknowledges the support of the FCT under Contract No. SFRH/BPD/69627/2010. Laboratoire Kastler Brossel is "Unité Mixte de Recherche du CNRS, de l' ENS et de l'UPMC" No. 8552. The LNHB authors acknowledge financial support for the determination of part of the data by the REXDAB collaboration that was initiated within the International Fundamental Parameter Initiative. We also acknowledge SOLEIL for the provision of synchrotron radiation facilities and would like to thank Paulo Da Silva and Pascal Mercere for assistance in using beamline "Metrologie."

[1] IUPAC, *Nomenclature System for x-ray Spectroscopy* (1999), http://old.iupac.org/reports/V/spectro/partVIII.pdf.
[2] R. W. Fink, R. C. Jopson, H. Mark, and C. D. Swift, Rev. Mod. Phys. **38**, 513 (1966).
[3] E. J. McGuire, Phys. Rev. A **2**, 273 (1970).
[4] D. L. Walters and C. P. Bhalla, Phys. Rev. A **3**, 1919 (1971).
[5] W. Bambynek, B. Crasemann, R. W. Fink, H. U. Freund, H. Mark, C. D. Swift, R. E. Price, and P. V. Rao, Rev. Mod. Phys. **44**, 716 (1972).
[6] C. P. Bhalla, J. Phys. B **3**, 916 (1970).
[7] M. H. Chen, B. Crasemann, and H. Mark, Phys. Rev. A **21**, 436 (1980).
[8] M. H. Chen, E. Laiman, B. Crasemann, M. Aoyagi, and H. Mark, Phys. Rev. A **19**, 2253 (1979).
[9] M. H. Chen, B. Crasemann, and H. Mark, Phys. Rev. A **21**, 449 (1980).
[10] M. H. Chen, B. Crasemann, and H. Mark, Phys. Rev. A **27**, 2989 (1983).
[11] B. Beckhoff and G. Ulm, Adv. X-Ray Anal. **44**, 349 (2001).
[12] Y. Ménesguen and M.-C. Lépy, Nucl. Instrum. Methods Phys. Res., Sect. B **268**, 2477 (2010).
[13] T. L. Hopman, C. M. Heirwegh, J. L. Campbell, M. Krumrey, and F. Scholze, X-Ray Spectrometry **41**, 164 (2012).
[14] K. R. Karim, J. Quant. Spectrosc. Radiat. Transfer **112**, 1026 (2011).
[15] C. Casteleiro, F. Parente, P. Indelicato, and J. P. Marques, Eur. Phys. J. D **56**, 1 (2010).
[16] J. Pahor, A. Kodre, M. Hribar, and A. Moljk, Z. Physik **221**, 490 (1969).
[17] W. Hartl and J. W. Hammer, Z. Phys. A **279**, 135 (1976).
[18] E. Casnati, A. Tartari, C. Baraldi, and G. Napoli, J. Phys. B **17**, 2413 (1984).
[19] G. Brunner, J. Phys. B **20**, 4983 (1987).
[20] J. K. Pious, K. M. Balakrishna, N. Lingappa, and K. Siddappa, J. Phys. B **25**, 1155 (1992).
[21] R. Durak and Y. Özdemr, Radiat. Phys. Chem. **61**, 19 (2001).
[22] M. O. Krause, J. Phys. Chem. Ref. Data **8**, 307 (1979).
[23] J. H. Hubbell, P. N. Trehan, N. Singh, B. Chand, D. Mehta, M. L. Garg, R. R. Garg, S. Singh, and S. Puri, J. Phys. Chem. Ref. Data **23**, 339 (1994).
[24] V. O. Kostroun, M. H. Chen, and B. Crasemann, Phys. Rev. A **3**, 533 (1971).
[25] D. R. Lide, *CRC Handbook of Chemistry and Physics 2009–2010*, A Ready-Reference Book of Chemical and Physical Data, 90th ed. (CRC Press, Boca Raton, FL, 2009).
[26] M. Jennewein, M. A. Lewis, D. Zhao, E. Tsyganov, N. Slavine, J. He, L. Watkins, V. D. Kodibagkar, S. O'Kelly, P. Kulkarni *et al.*, Clinical Cancer Research **14**, 1377 (2008).
[27] J. Desclaux, Comput. Phys. Commun. **9**, 31 (1975).
[28] P. Indelicato and J. Desclaux, MCDFGME, *A Multi-Configuration Dirac Fock and General Matrix Elements Program* (2007), http://dirac.spectro.jussieu.fr/mcdf.
[29] P. Indelicato and J. P. Desclaux, Phys. Rev. A **42**, 5139 (1990).
[30] P. Indelicato, Phys. Rev. A **51**, 1132 (1995).
[31] P. Indelicato, Phys. Rev. Lett. **77**, 3323 (1996).
[32] P. Indelicato, O. Gorveix, and J. P. Desclaux, J. Phys. B **20**, 651 (1987).
[33] O. Gorceix, P. Indelicato, and J. P. Desclaux, J. Phys. B **20**, 639 (1987).
[34] P. Indelicato, Nucl. Instrum. Methods Phys. Res., Sect. B **31**, 14 (1988).
[35] J. P. Santos, G. C. Rodrigues, J. P. Marques, F. Parente, J. P. Desclaux, and P. Indelicato, Eur. Phys. J. D **37**, 201 (2006).
[36] P.-O. Löwdin, Phys. Rev. **97**, 1474 (1955).

[37] J. P. Santos, J. P. Marques, F. Parente, E. Lindroth, P. Indelicato, and J. P. Desclaux, J. Phys. B **32**, 2089 (1999).
[38] J. M. Sampaio, F. Parente, P. Indelicato, and J. P. Marques, J. Phys. B **46**, 065001 (2013).
[39] A. M. Costa, M. C. Martins, J. P. Santos, P. Indelicato, and F. Parente, At. Data Nucl. Data Tables **79**, 223 (2001).
[40] R. D. Deslattes, E. Kessler, P. Indelicato, L. de Billy, E. Lindroth, and J. Anton, Rev. Mod. Phys. **75**, 35 (2003).
[41] Y. Ménesguen and M.-C. Lépy, X-Ray Spectrom. **40**, 411 (2011).
[42] J. L. Campbell, G. Cauchon, T. Lakatos, M.-C. Lépy, L. McDonald, T. Papp, J. Plagnard, P. Stemmler, and W. J. Teesdale, J. Phys. B **31**, 4765 (1998).
[43] D. C. Creagh and J. H. Hubbell, Acta Crystallogr. **43**, 102 (1987).
[44] B. Nordfors, Arkiv für Fysik **18**, 37 (1960).
[45] R. Brun and F. Rademakers, Nucl. Instrum. Methods Phys. Res. A **389**, 81 (1997).
[46] H. Ruellan, M.-C. Lépy, M. Etcheverry, J. Plagnard, and J. Morel, Nucl. Instr. Methods A **369**, 651 (1996).
[47] C. T. Chantler, J. Phys. Chem. Ref. Data **24**, 71 (1995).
[48] M. Berger, J. Hubbell, S. Seltzer, J. Chang, J. Coursey, R. Sukumar, and D. Zucker, XCOM: Photon Cross Section Database (version 1.3) 2005, National Institute of Standards and Technology, Gaithersburg, MD.